Pharm Res (2013) 30:70–80
DOI 10.1007/s11095-012-0850-1

RESEARCH PAPER

# Detection of Cocrystal Formation Based on Binary Phase Diagrams Using Thermal Analysis

Hiroyuki Yamashita • Yutaka Hirakura • Masamichi Yuda • Toshio Teramura • Katsuhide Terada

Received: 18 April 2012 / Accepted: 31 July 2012 / Published online: 21 August 2012


## ABSTRACT

***Purpose*** Although a number of studies have reported that cocrystals can form by heating a physical mixture of two components, details surrounding heat-induced cocrystal formation remain unclear. Here, we attempted to clarify the thermal behavior of a physical mixture and cocrystal formation in reference to a binary phase diagram.

***Methods*** Physical mixtures prepared using an agate mortar were heated at rates of 2, 5, 10, and 30°C/min using differential scanning calorimetry (DSC). Some mixtures were further analyzed using X-ray DSC and polarization microscopy.

***Results*** When a physical mixture consisting of two components which was capable of cocrystal formation was heated using DSC, an exothermic peak associated with cocrystal formation was detected immediately after an endothermic peak. In some combinations, several endothermic peaks were detected and associated with metastable eutectic melting, eutectic melting, and cocrystal melting. In contrast, when a physical mixture of two components which is incapable of cocrystal formation was heated using DSC, only a single endothermic peak associated with eutectic melting was detected.

***Conclusion*** These experimental observations demonstrated how the thermal events were attributed to phase transitions occurring in a binary mixture and clarified the relationship between exothermic peaks and cocrystal formation.

H. Yamashita (✉) • Y. Hirakura • M. Yuda • T. Teramura
Analysis and Pharmacokinetics Research Labs, Astellas Pharma Inc.
21, Miyukigaoka
Tsukuba, Ibaraki 350-8585, Japan
e-mail: hiroyuki.yamashita@astellas.com

H. Yamashita • K. Terada
Faculty of Pharmaceutical Science, Toho University
2-2-1, Miyama
Funabashi, Chiba 274-8510, Japan

**KEY WORDS** cocrystal formation · DSC · eutectic · exothermic · physical mixture

## INTRODUCTION

Cocrystal is defined as a crystalline material which comprises two or more unique solid components in a stoichiometric ratio (1–3). Interest in cocrystals in the pharmaceutical industry has increased in recent years, as these crystals may improve physicochemical properties of drug candidate compounds, including solubility (4–6), physical stability (7,8), mechanical properties (9,10), and bioavailability (11). A number of methods for preparing cocrystals have been reported, such as solution crystallization (12–14), slurry conversion (15,16), evaporation (17,18), co-grinding (8,19–21), ultrasound crystallization (22), and heat-induced crystallization (23–25). Heat-induced cocrystallization in particular is drawing attention because this method does not need organic solvents, presenting a green alternative to presently available methods, and also spares the time-consuming work of solubility determination for solution crystallization. However, the details of such heat-induced cocrystallzation have not yet been clarified.

Binary phase diagrams of combinations that are capable of cocrystal formation are shown in Fig. 1 (26). Of the two such combinations known, one is characterized by a so-called congruent melting point, while the other involves an incongruent melting point. In the pharmaceutical sciences, congruent melting has been reported with a number of combinations including benzophenone–diphenylamine(23), vanillin–p-anisidine

(27), o-phenylenediamine–benzoin(28), and benzidine-p-nitrophenol(29) while incongruent melting has been rarely described(30) with examples including combinations of phenobarbitone-urea(31) and paracetamol-phenazone(32). Equilibrium behavior derived from the phase diagrams is described as follows: In a congruent melting system (Fig. 1a), when a physical mixture of molar ratio 1:1 is heated, all of component A and part of component B melt at the metastable eutectic temperature ($T_{m\text{-}E}$), forming a cocrystal which then melts at the melting point ($T_c$). When DSC is used, one clear endothermic peak associated with metastable eutectic melting followed by one exothermic peak associated with cocrystal formation should be observed at $T_{m\text{-}E}$, while another endothermic peak associated with cocrystal melting should be detected at $T_C$ (congruent melting point=cocrystal melting point). In an incongruent melting system (Fig. 1b), when a physical mixture of molar ratio 1:1 is heated, all of component A and part of component B melt at the metastable eutectic temperature ($T_{m\text{-}E}$), forming a cocrystal—behavior which is the same as that in a congruent melting system. Notably, the cocrystal melts and component B recrystallizes at the incongruent melting point or peritectic point ($T_P$) until a liquid of composition at P in Fig. 1b is reached, and component B then melts gradually at temperatures higher than $T_P$. When DSC is used, a clear endothermic peak associated with metastable eutectic melting followed by an exothermic peak associated with cocrystal formation should be observed at $T_{m\text{-}E}$, while another endothermic peak associated with cocrystal melting and another exothermic peak associated with recrystallization of component B at $T_P$, followed by a broad endothermic deflection at temperatures above $T_P$, should also be observed.

The binary phase diagram of a combination incapable of cocrystal formation is shown in Fig. 2 (26). The equilibrium behavior with this combination is described as follows: When a physical mixture of molar ratio 1:1 is heated, component A and part of component B melt at the eutectic temperature ($T_E$), with the rest of solid component B melting gradually with increasing temperatures. When DSC is used, one clear endothermic peak at $T_E$ followed by a broad endothermic deflection at temperatures above $T_E$ should be observed.

When comparing physical mixtures that are capable and incapable of cocrystal formation, we note that only the former involves exothermic events. When a physical mixture capable of cocrystal formation is heated, one or two exothermic peaks are rationally detected on a thermal trace. While the equilibrium behavior of a binary system has been described in a phase diagram, it has not always been easy to reproduce. Here, we subjected compounds to DSC, powder X-ray diffractometry (PXRD), X-ray DSC, and polarization microscopy, and addressed the kinetics as well as the equilibrium behavior. The impacts of cogrinding on the equilibrium and kinetics were also examined for detection of cocrystal formation.

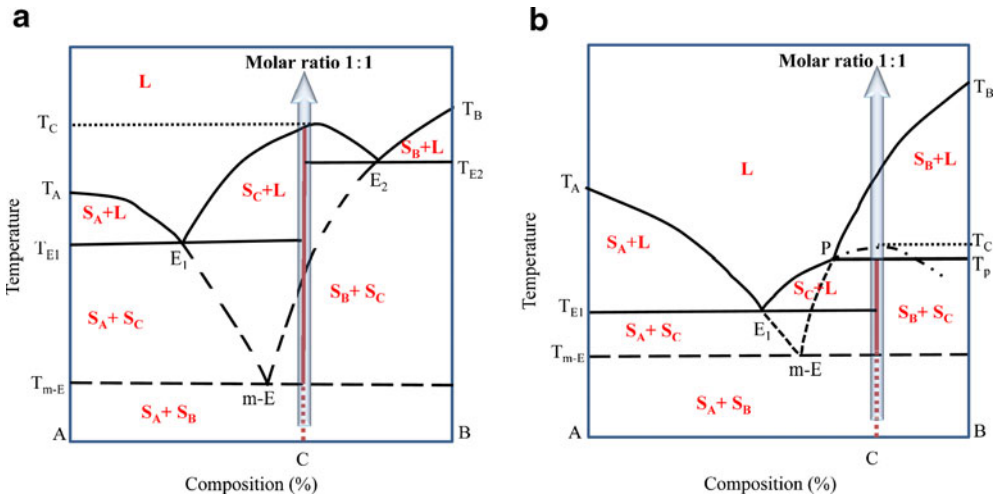


**Fig. 1** Binary phase diagrams of combinations capable of cocrystal formation. (**a**) Congruent melting system, (**b**) incongruent melting system. L, liquid; $S_A$, solid of component A; $S_B$, solid of component B; $S_C$, cocrystal; E, eutectic point; m-E, metastable eutectic point; P, peritectic point; $T_{m\text{-}E}$, metastable eutectic temperature; $T_E$, eutectic temperature; $T_P$, peritectic temperature; $T_A$, melting temperature of component A; $T_B$, melting temperature of component B; $T_C$, melting temperature of cocrystal.

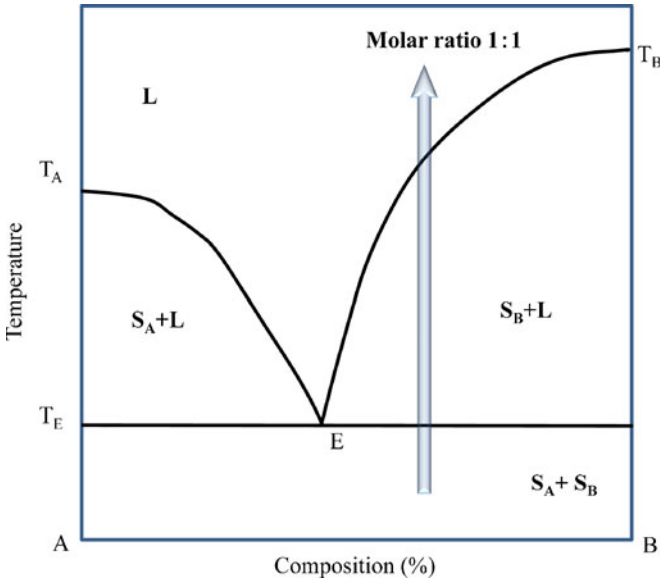


**Fig. 2** Binary phase diagram of a combination incapable of cocrystal formation. L, liquid; $S_A$, solid of component A; $S_B$, solid of component B; E, eutectic point; $T_E$, eutectic temperature; $T_A$, melting temperature of component A; $T_B$, melting temperature of component B.

## MATERIALS AND METHODS

### Materials

Indomethacin (IND), piroxicam (PIR), theophylline (THE), and carbamazepine (CAR) were purchased from Sigma Aldrich (St. Louis, MO, USA); saccharin, urea, caffeine, benzoic acid, and fumaric acid were obtained from Wako Pure Chemical Industries (Osaka, Japan); and nicotinamide and salicylic acid were purchased from Nacalai Tesque (Kyoto, Japan). All other compounds and solvents were of analytical grade, obtained from Kanto Chemical (Tokyo, Japan), and used as received.

### Grinding

Twenty milligrams of each active pharmaceutical ingredient (API) and stoichiometric (1:1) coformer (CCF) were weighed, respectively, and mixed in a 2-mL vial. After mixing, the compound was ground manually in an agate mortar for 30 s.

### Differential Scanning Calorimetry

Thermal analysis of physical mixtures was performed using a TA Q1000 DSC instrument with a refrigerated cooling system (TA Instruments, New Castle, DE, USA). Temperature calibration was carried out using an indium metal standard supplied with the instrument. Physical mixtures were weighed out (1.5–2.5 mg) in aluminum pans and analyzed from 25 to 250°C at heating rates of 2, 5, 10, and 30°C/min using a similar empty pan as a reference. An inert atmosphere was maintained in the calorimeter by purging nitrogen gas at a flow rate of 50 mL/min.

### X-Ray DSC

Simultaneous measurement of powder X-ray diffraction data and DSC data was carried out using a SmartLab system (X-ray wavelength: 0.154 nm Cu source, voltage: 45 kV, current: 200 mA) with a DSC attachment (Rigaku, Tokyo, Japan) and a D/Tex Ultra adapted as a detector. Physical mixtures were weighed out (1.5–2.5 mg) in aluminum pans and analyzed from 25 to 250°C at a heating rate of 2°C/min using a similar empty pan as a reference. X-ray diffraction data were collected at a scan rate of 20°/min over a 2θ range of 8° to 30°.

### Preparation of Carbamazepine (+)-Camphoric Acid Cocrystal

Ten milligrams of carbamazepine (0.0423 mmol) and 8.47 mg (+)-camphoric acid (0.0423 mmol) were weighed out and then mixed and stirred in 0.1 mL tetrahydrofuran/heptane (1:1) solution in a 2-mL vial for 24 h at room temperature. Powder was collected from the slurry solution using filtration and dried under reduced pressure at 50°C using a vacuum drying oven DP43 (Yamato Scientific Co., Ltd., Tokyo, Japan)

### Powder X-Ray Diffraction

PXRD patterns (X-ray wavelength: 0.154 nm Cu source, voltage: 50 kV, current: 300 mA) of single-phase crystals were confirmed using a TTR II (Rigaku). Data were collected at a scan rate of 4°/min over a 2θ range of 8° to 30°.

### Polarization Microscopy

Microscopy observation was performed using an ECLIPSE E600-POL (Nikon Corporation, Tokyo, Japan). Photoshop Elements 8 (Adobe, San Jose, CA, USA) was used for picture processing.

## RESULTS AND DISCUSSION

### Detection of An Exothermic Peak Associated with Cocrystal Formation

Physical mixtures were prepared, coground, and analyzed using DSC at heating rates of 2, 5, 10, and 30°C/min. The thermal behavior of a physical mixture of caffeine and salicylic acid is shown in Fig. 3. Although findings showed that behavior did depend on heating rate, a clear endothermic peak was observed at 120°C, immediately followed by an exothermic peak, suggesting cocrystal formation. The second endothermic peak was observed at 142°C, which is the melting point of the cocrystal (33). This behavior was common at all heating rates.

The thermal behavior of a physical mixture of THE and nicotinamide is shown in Fig. 4. An endothermic peak was observed at 124°C, immediately followed by an exothermic peak, again suggesting cocrystal formation. The second peak was detected at 172°C, which is the melting point of the cocrystal (34). This behavior was common at all heating rates.

The thermal behavior of a physical mixture of caffeine and nicotinamide, which is reported to be incapable of cocrystal formation (33), is shown in Fig. 5. A single sharp endothermic peak observed at 119°C seemed to be associated with eutectic melting. No exothermic peaks were detected at any heating rates.

Experimental results are summarized in Table I. Of the 20 physical mixtures prepared for pulverization and analysis using a DSC instrument, 17 had been reported as combinations capable of cocrystal formation (7,18,33–37). In all 17 of these combinations, an exothermic peak associated with cocrystal formation was confirmed. Since phase transitions between polymorphs or between anhydrates and hydrates can appear as exothermic peaks, we avoided using compounds with a large exothermic peak in the absence of a CCF in the present study. In contrast to the above findings, no exothermic peaks were observed with the three physical mixtures for which no cocrystals had been previously reported (CAR-hippuric acid, caffeine-nicotinamide, and caffeine-urea) (33). Taken together, these observations indicate that when a physical mixture is heated, cocrystal formation is detected as an exothermic peak as predicted theoretically from the binary phase diagrams, suggesting the ability to predict cocrystal formation based on presence of an exothermic peak in DSC.

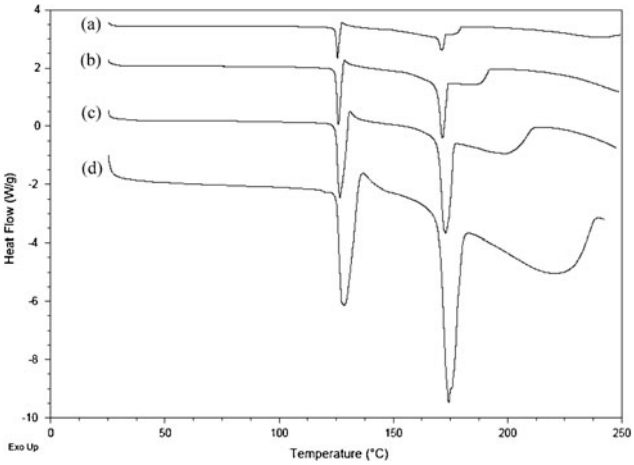


**Fig. 4** Thermal behavior of a physical mixture of theophylline and nicotinamide. Heating rates of (**a**) 2°C/min, (**b**) 5°C/min, (**c**) 10°C/min, and (**d**) 30°C/min.

### Detection of Several Endothermic Peaks

Since several endothermic peaks were observed on a DSC trace as well as an exothermic peak in some cases, we tried to

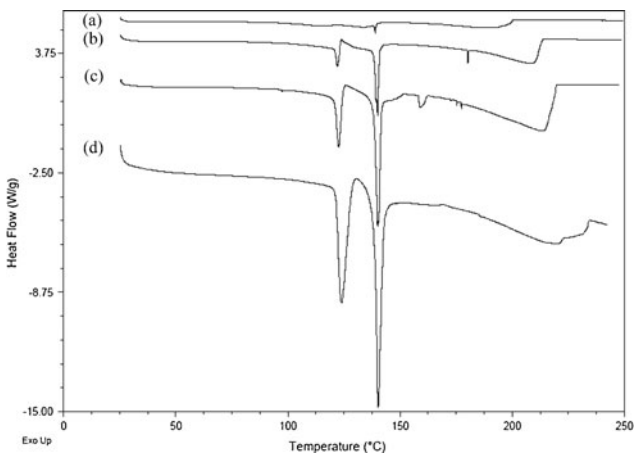


**Fig. 3** Thermal behavior of a physical mixture of caffeine and salicylic acid. Heating rates of (**a**) 2°C/min, (**b**) 5°C/min, (**c**) 10°C/min, and (**d**) 30°C/min.

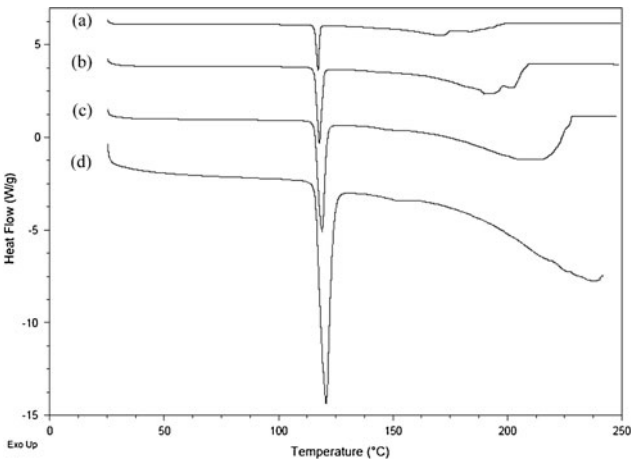


**Fig. 5** Thermal behavior of a physical mixture of caffeine and nicotinamide. Heating rates of (**a**) 2°C/min, (**b**) 5°C/min, (**c**) 10°C/min, and (**d**) 30°C/min.

**Table I** Summary of Detection of Exothermic Peaks in DSC

| API | MP (°C) | CCF | MP (°C) | Cocrystal reported? [a] | Cocrystal MP (°C) | Exothermic peak (°C) [b] |
|---|---|---|---|---|---|---|
| Indomethacin | 162 | Saccharin | 225–227 | Yes (18) | 182 | 153 |
| Piroxicam | 198–200 | Saccharin | 225–227 | Yes (35) | 220 | 171 |
| Theophylline | 272 | Glutaric acid | 98 | Yes (7) | 118 | 102 |
| | | Nicotinamide | 128 | Yes (34) | 172 | 127 |
| | | Saccharin | 225–227 | Yes (33) | 207 | 186 |
| | | Urea | 135 | Yes (33) | 205 | 137 |
| Caffeine | 142 | Glutaric acid | 98 | Yes (33) | 96 | 85 |
| | | Saccharin | 225–227 | Yes (33) | 155 | 150 |
| | | Salicylic acid | 159 | Yes (33) | 142 | 124 |
| | | Nicotinamide | 128 | No (33) | – | N.D. |
| | | Urea | 133–135 | No (33) | – | N.D. |
| Carbamazepine | 191 | Benzoic acid | 122 | Yes (36) | 113 | 78 |
| | | (+)-Camphor acid | 186 | Yes (36) | 156 | 119 |
| | | Fumaric acid | 200 | Yes (36) | 189 | 165 |
| | | Glutaric acid | 98 | Yes (36) | 125 | 97 |
| | | L-Tartaric acid | 169 | Yes (36) | 160 | 133 |
| | | Nicotinamide | 128 | Yes (37) | 157 | 127 |
| | | Saccharin | 225 | Yes (36) | 174 | 128 |
| | | Succinic acid | 187 | Yes (36) | 189 | 179 |
| | | Hippuric acid | 187 | No (33) | - | N.D. |

[a] Figures in parentheses indicate reference numbers

[b] The temperatures of the major exothermic peaks are shown

*API* active pharmaceutical ingredient, *CCF* coformer, *MP* melting point, *N.D.* not detected

relate those peaks to the phase diagrams. The thermal behavior of a physical mixture of CAR and (+)-camphoric acid is shown in Fig. 6. At a heating rate of 2°C/min, broad endothermic and exothermic peaks were observed at approximately 110°C, with 3 other endothermic peaks detected at 140, 148, and 151°C (1 peak each). Four endothermic peaks were observed in total (arrows in Fig. 6). To examine what occurred at these temperatures, cocrystal of CAR and (+)-camphoric acid was prepared from solution for X-ray DSC analysis. PXRD data of (+)-camphoric acid, CAR, and the prepared cocrystal were collected at 25°C after grinding. The PXRD patterns are shown in Fig. 7. Typical diffraction peaks of each compound were identified (colored arrows); diffraction patterns of CAR, (+)-camphoric acid, and the cocrystal remained unchanged from 25 to 150°C (data not shown).

X-ray DSC analysis of a physical mixture of CAR and (+)-camphoric acid is shown in Fig. 8. The sample was heated at a rate of 2°C/min. The first endothermic peak at 110°C was shown to be associated with metastable eutectic melting of CAR and (+)-camphoric acid, as new typical diffraction peaks of cocrystal appeared with an exothermic peak (2θ=10.5°, 13.7°, 14.2°, 17.5°, 18.1°, and 21.4°). The second endothermic peak at 140°C was suggested to be associated with eutectic melting of CAR and cocrystal at $T_{E1}$, as typical diffraction peaks of CAR disappeared at 13.3°, 15.9°, 18.7°, and 19.5°, while those of (+)-camphoric acid remained at 14.0°, 16.8°, and 17.2°. Since typical diffraction peaks of (+)-camphoric acid disappeared at 148°C, the third subtle endothermic peak was associated

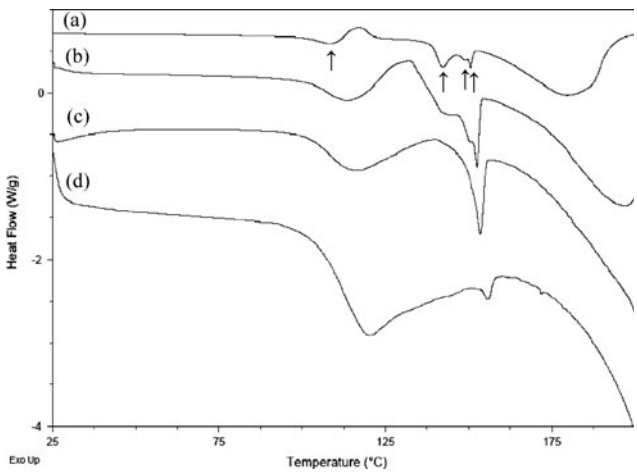


**Fig. 6** The thermal behavior of a physical mixture of carbamazepine and (+)-camphoric acid. Heating rates of (**a**) 2°C/min, (**b**) 5°C/min, (**c**) 10°C/min, and (**d**) 30°C/min.

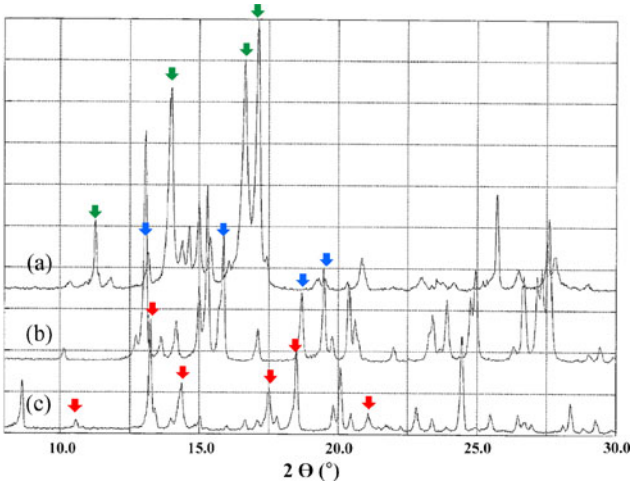


**Fig. 7** PXRD patterns of (+)-camphor acid, carbamazepine (CAR), and cocrystal prepared from solution. (**a**) (+)-camphor acid, (**b**) carbamazepine, and (**c**) cocrystal. Analyzed at 25°C after grinding. Red arrows indicate typical diffraction peaks of the cocrystal, green ones those of (+)-camphoric acid, and blue ones those of the stable form of CAR at low temperatures.

with eutectic melting of (+)-camphoric acid and cocrystal at $T_{E2}$. The final endothermic peak at 151°C was associated with cocrystal melting at $T_c$. The above observations were considered to be congruent melting behavior, as no new diffraction peaks appeared after the cocrystal melted.

In a binary system capable of cocrystal formation, both individual components melt and cocrystal forms at the metastable eutectic point, and an endothermic peak immediately followed by an exothermic peak will be observed around that temperature. In a congruent melting system, the cocrystal melts at the melting point, at which a single endothermic peak will be observed, with two endothermic peaks in total typically observed on a DSC curve. In some cases, however, physical shielding due to cocrystal formation occurs, resulting in several separate endothermic events (Fig. 9). When it forms at the metastable eutectic temperature, the cocrystal interferes with contact between components A and B at the interface. Studies using microscopy have reported that cocrystal forms from a contact surface between two components (11,23). Due to the physical shielding, the metastable eutectic melting of components A and B and subsequent cocrystal formation are partially hindered at $T_{m\text{-}E}$. When heated, cocrystal and the remaining component A melt at the eutectic temperature ($T_{E1}$) while cocrystal and the remaining component B melt at the second eutectic temperature ($T_{E2}$). Cocrystal melts at its melting point ($T_C$). A total of four endothermic peaks can thus be observed on a DSC curve, as shown in Fig. 6. In principle, a maximum of three exothermic peaks may appear due to cocrystallization following the endothermic events in these cases because cocrystals can form at $T_{E1}$ and $T_{E2}$ as well as $T_{m\text{-}E}$ (Fig. 9). Solid component B is dissolved into

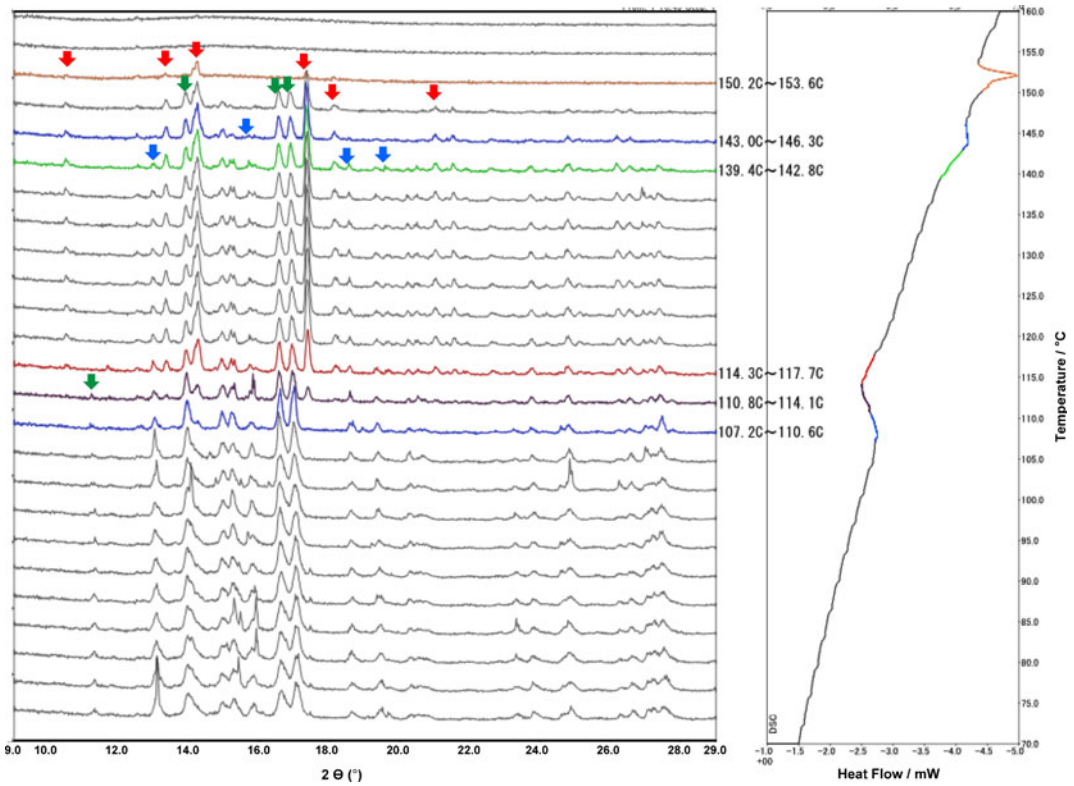


**Fig. 8** X-ray DSC analysis of a physical mixture of carbamazepine (CAR) and (+)-camphoric acid. Red arrows indicate typical diffraction peaks of the cocrystal, green ones those of (+)-camphoric acid, and blue ones those of the stable form of CAR at low temperatures as in Fig. 7.

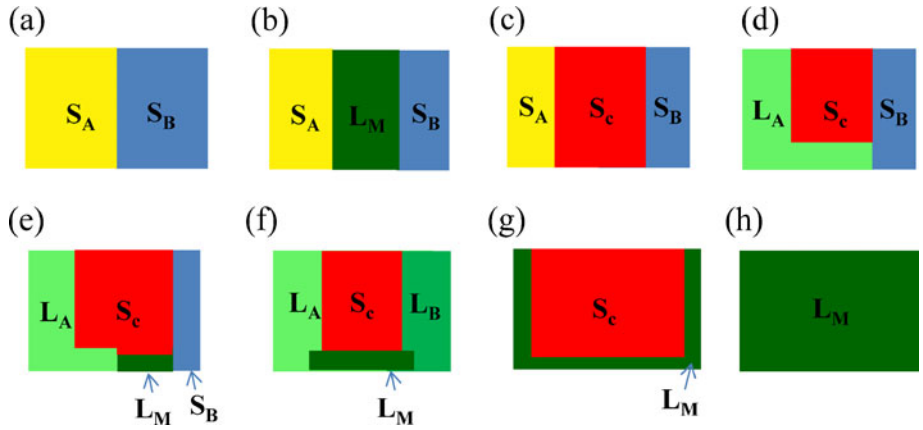


**Fig. 9** Schematic illustration of thermal events observed with a congruent melting system at $T_{m\text{-}E}$, $T_{E1}$, $T_{E2}$, and $T_C$. $S_A$, solid of component A; $S_B$, solid of component B; $S_C$, cocrystal; $L_A$, A-rich liquid; $L_B$, B-rich liquid; $L_M$, liquid of cocrystal forming composition; $T_{m\text{-}E}$, metastable eutectic temperature; $T_{E1}$, eutectic temperature 1; $T_{E2}$, eutectic temperature 2; $T_C$, melting point of cocrystal. (**a**) $S_B$ contacts with $S_A$ in a physical mixture. (**b**) Eutectic melting of $S_A$ and $S_B$ occurs at $T_{m\text{-}E}$ to form $L_M$. (**c**) Cocrystal ($S_C$) forms from $L_M$ to hinder the contact of $S_A$ with $S_B$. (**d**) Eutectic melting of $S_A$ and $S_C$ occurs at $T_{E1}$ and $L_A$ appears. (**e**) $S_B$ contacts with and dissolves into $L_A$ to form $L_M$ to induce cocrystallization. (**f**) Eutectic melting of $S_B$ and $S_C$ occurs at $T_{E2}$ and $L_B$ appears. (**g**) $L_A$ and $L_B$ are mixed to each other to form $L_M$ to induce cocrystallization. (**h**) Cocrystal melts at $T_C$.

component A-rich eutectic mixture generated at $T_{E1}$ to create an unstable liquid of cocrystal-forming composition, which then results in cocrystal formation, occurring as an exothermic peak. As the cocrystallization is incomplete, component B-rich eutectic mixture generated at $T_{E2}$ is mixed with the remaining liquid to create an unstable liquid whose composition is more suitable (near equimolar ratio) for cocrystal formation, which again occurs as an exothermic peak.

In an incongruent melting system, a total of three endothermic peaks are observed ($T_{m\text{-}E}$, $T_{E1}$, and $T_P$). While exothermic events always originate from cocrystallization in a congruent melting system, exothermic events in an incongruent melting system occur as component B recrystallizes at the peritectic temperature ($T_P$). Accordingly, exothermic peaks due to a physical event other than cocrystal formation can be observed in this melting system. This remains compatible with the association of the emergence of an exothermic peak with cocrystal formation capability of a physical mixture, because it always holds true that an incongruent melting system is capable of cocrystal formation.

## Dependence on Heating Rates and Cocrystal Formation Kinetics

According to binary phase diagrams, an exothermic event associated with cocrystal formation should always occur when a physical mixture capable of cocrystal formation is heated. Indeed, exothermic peaks were observed on DSC curves of various physical mixtures in the present study as noted above. However, exothermic peaks were not observed at certain heating rates in some physical mixtures.

The thermal behavior of a physical mixture of PIR and saccharin is shown in Fig. 10. Obvious endothermic and exothermic peaks were observed at around 170°C at heating rates of 2 and 5°C/min, and an obvious endothermic peak and broad exothermic peak were detected at a heating rate of 10°C/min. Remarkably, only an endothermic peak, with no exothermic peaks, was observed at around 170°C at a relatively fast heating rate of 30°C/min.

The thermal behavior of a physical mixture of CAR and nicotinamide is shown in Fig. 11. Sharp and large endothermic and exothermic peaks were observed at approximately 110°C at a heating rate of 30°C/min. Smaller and less obvious endothermic and exothermic peaks were confirmed at a heating rate of 10°C/min. In marked contrast, no endothermic or exothermic peaks were observed at around 110°C at a relatively slow heating rate of 2 and 5°C/min.

X-ray DSC analysis of a physical mixture of CAR and nicotinamide was shown in Fig. 12. The sample was heated

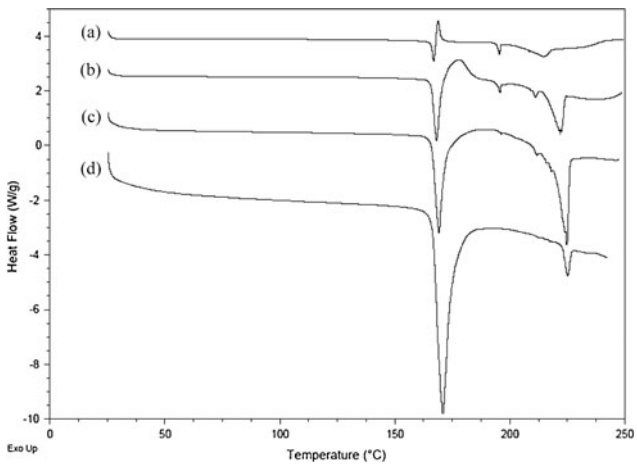


**Fig. 10** The thermal behavior of a physical mixture of piroxicam and saccharin. Heating rates of (**a**) 2°C/min, (**b**) 5°C/min, (**c**) 10°C/min, and (**d**) 30°C/min.

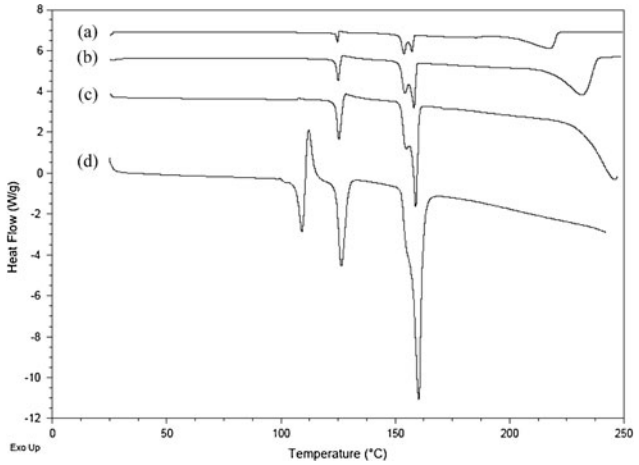


**Fig. 11** The thermal behaviors of a physical mixture of carbamazepine and nicotinamide. Heating rates of (**a**) 2°C/min, (**b**) 5°C/min, (**c**) 10°C/min, and (**d**) 30°C/min.

at a rate of 2°C/min, and diffraction peaks of cocrystal started to appear at 8.9°, 10.0°, 13.4°, 17.8°, and 22.9° at temperatures exceeding 110°C, suggesting that this is the metastable eutectic point ($T_{m\text{-}E}$) of the binary system. A large endothermic peak followed by an exothermic peak was observed at approximately 125°C. The exothermic heat likely originated from cocrystallization following the eutectic melting of nicotinamide and cocrystal at $T_{E1}$ (Fig. 9), given that the diffraction peaks of nicotineamide disappeared at 14.8°, 22.1°, and 25.7° while those of the cocrystal started to grow in peak height at this temperature.

Whether an endothermic or an exothermic peak is observed in DSC depends on differences in cocrystal formation kinetics as well as heating rates. Cocrystal formation (based on nucleation and growth) can occur at any time after eutectic melting. In general, when cocrystal forms at temperatures exceeding the metastable eutectic melting ($T_{m\text{-}E}$) or eutectic melting ($T_{E1}$ or $T_{E2}$) point, both endothermic and exothermic peaks may be observed on a DSC curve. When eutectic melting ($T_{m\text{-}E}$, $T_{E1}$, or $T_{E2}$) and cocrystallizaton occur almost simultaneously, the endothermic and exothermic peaks can cancel each other, rendering neither observable. In terms of heating rate, temperature resolution of DSC is better at a slower heating rate than a faster one. It is therefore reasonable that a slower heating rate has an advantage in coping with the cancellation of exothermic and endothermic heats.

Temperature resolution appeared to play a major role in cancellation as shown in Fig. 10, where the exothermic peak due to cocrystallization was overlapped and obscured by the endothermic peak due to metastable eutectic melting at a higher heating rate. In striking contrast, a heating rate of 30°C/min was more useful than one of 2°C/min for detecting both an exothermic and endothermic peak at approximately 110°C in Fig. 11. One possible explanation for this

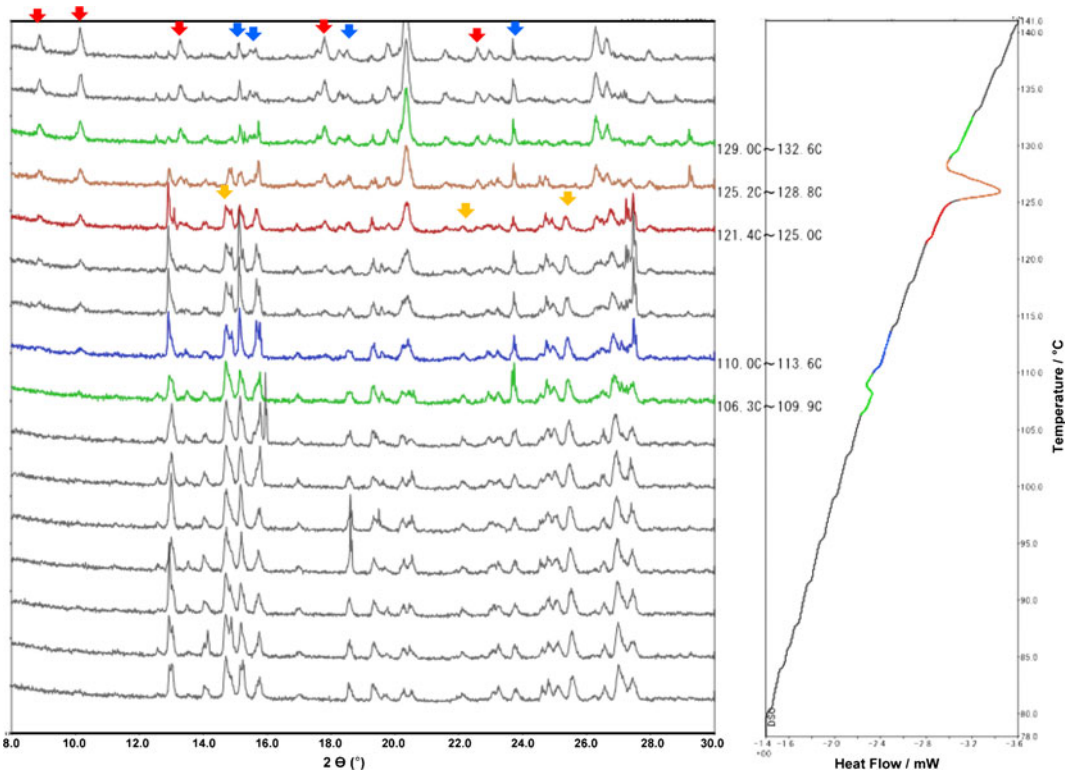


**Fig. 12** X-ray DSC analysis of a physical mixture of carbamazepien (CAR) and nicotinamide. Red arrows are typical diffraction peaks of the cocrystal, yellow ones those of nicotinamide, and blue ones those of the stable form of CAR at low temperature.

striking observation is that metastable eutectic melting and cocrystallization were liable to kinetic hindrance (including physical shielding) at a lower heating rate because cocrystallization occurred considerably at $T_{E1}$ as well as $T_{m\text{-}E}$ as shown in Fig. 12. Alternatively, endothermic and exothermic heats at 110°C tended to be cancelled out at slower heating rates, as these thermal events occurred almost simultaneously. A third possible explanation is that both thermal events may have been at or below the detection sensitivity level at relatively low heating rates. As such, it is difficult to conclude the optimum heating rate for detecting exothermic peaks associated with cocrystal formation on a DSC curve. No perfect heating rate exists, and variable heating rates should therefore be adopted.

### Grinding Using An Agate Mortar

In the present study, grinding using an agate mortar was conducted before analysis. Grinding greatly influenced the thermal behavior of physical mixtures; results of microscopic observation and thermal behavior before and after grinding are shown in Figs. 13 and 14. While the combination of CAR and fumaric acid is known to be capable of cocrystal formation, no exothermic peak was observed on DSC curves without grinding (Fig. 13C). With grinding, however, both endothermic and exothermic peaks associated with eutectic melting and cocrystal formation were observed clearly at approximately 170°C (Fig. 13D). Conversely, while the combination of CAR and hippuric acid is believed to be incapable of cocrystal formation, several endothermic peaks were observed on DSC curves without grinding (Fig. 14C). With grinding, however, a single endothermic peak associated with eutectic melting was detected (Fig. 14D). These marked differences in thermal behavior based on grinding are attributed to the differences in particle size and contact area. The particle size in the physical mixture of CAR and fumaric acid was reduced from more than 100 μm in diameter before grinding to less than 30 μm in diameter after. Differences in particle

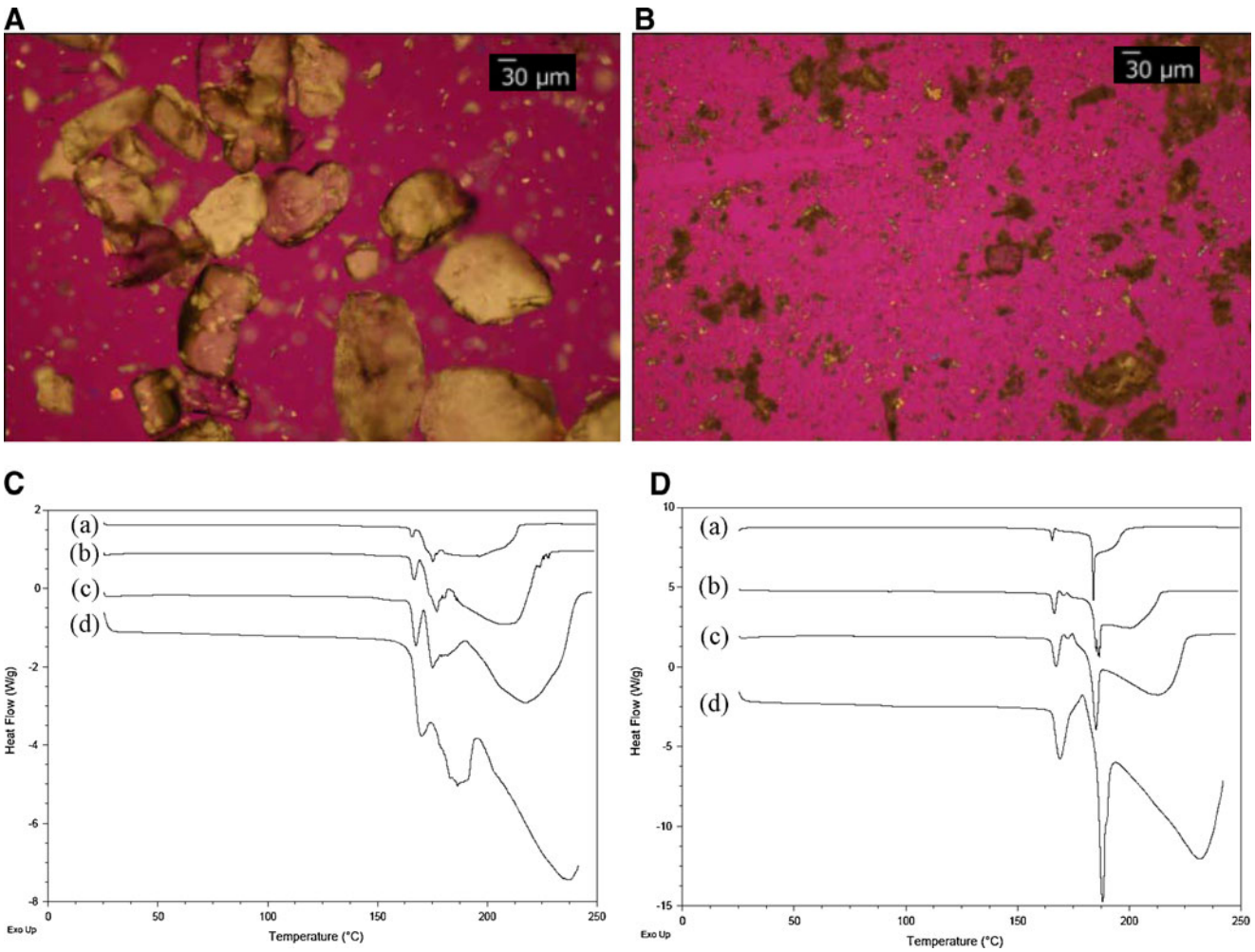


**Fig. 13** The microscopic observation and thermal behavior of a physical mixture of carbamazepine and fumaric acid. Polarization microscopic picture before (**A**) and after (**B**) grinding. Thermal behavior before (**C**) and after (**D**) grinding. Heating rates of (**a**) 2°C/min, (**b**) 5°C/min, (**c**) 10°C/min, and (**d**) 30°C/min.

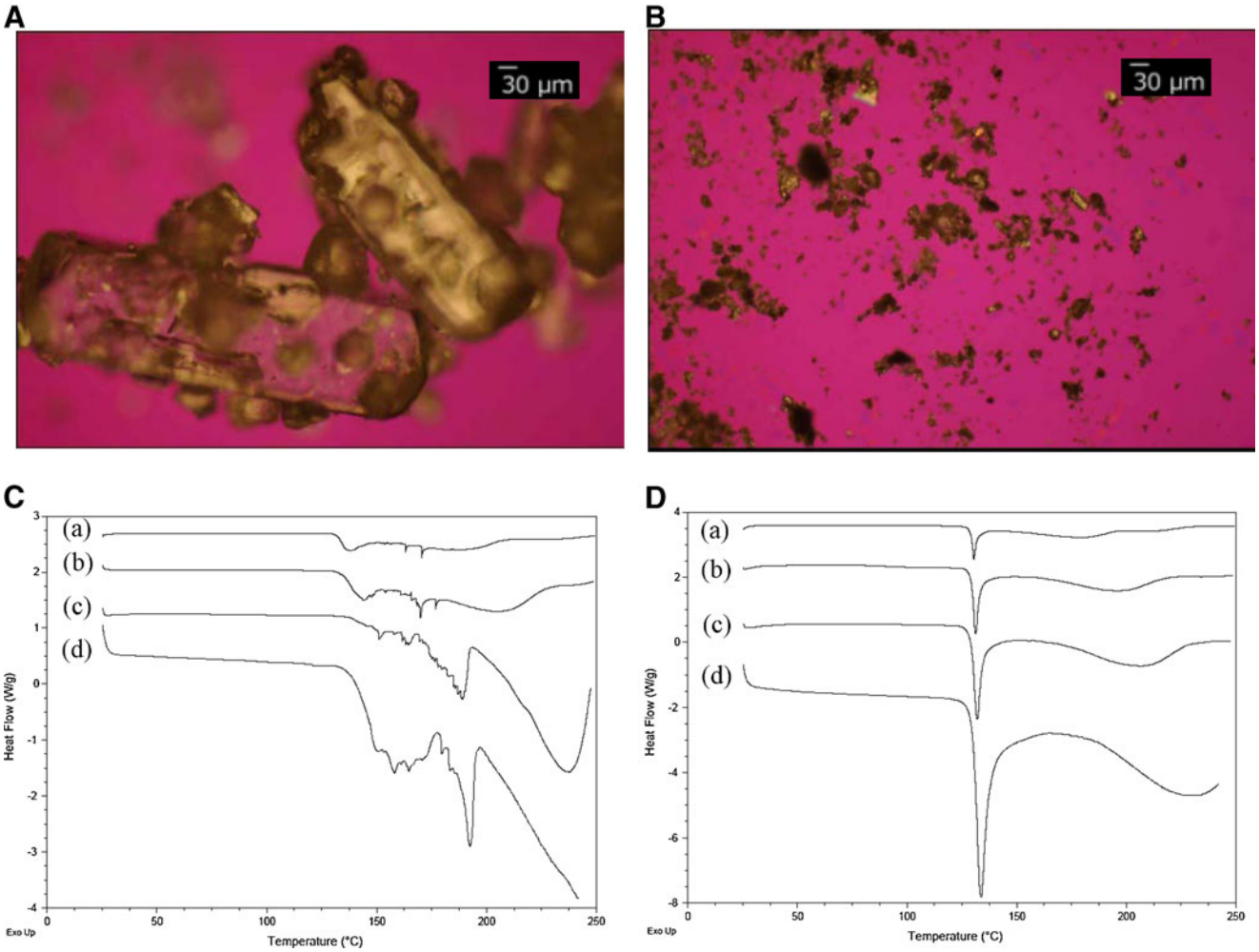


**Fig. 14** The microscopic observation and thermal behavior of a physical mixture of carbamazepine and hippuric acid. Polarization microscopic picture before (**A**) and after (**B**) grinding. Thermal behavior before (**C**) and after (**D**) grinding. Heating rates of (**a**) 2°C/min, (**b**) 5°C/min, (**c**) 10°C/min, and (**d**) 30°C/min.

size before and after grinding were even more pronounced in the physical mixture of CAR and hippuric acid. Ensuring that fine particles are mixed homogeneously is crucial to reproducing the typical thermal behavior noted in the binary phase diagrams.

Grinding may promote cocrystal formation or reduce crystallinity. A previous study reported that cocrystal formed during grinding (by auto-mill, 30 min) in a physical mixture of CAR and saccharin (38). Since grinding for 30 s in an agate mortar was used as a standard procedure in the present study, no cocrystal formation or reduction in crystallinity was observed (data not shown). These differences between the present and previous study are likely ascribed to differences in the strength and duration of grinding.

## CONCLUSION

When a physical mixture of two components capable of cocrystal formation was heated using DSC, an exothermic peak associated with cocrystal formation was detected. In some combinations, several endothermic peaks were detected and associated with metastable eutectic melting, eutectic melting, and cocrystal melting. In contrast, when a physical mixture of two components incapable of cocrystal formation was heated using DSC, one endothermic peak associated with eutectic melting was detected. Using homogeneously-mixed fine particles in our study was crucial to eliciting the behavior noted in the binary phase diagrams. Although cancelation of endothermic and exothermic peaks occurred depending on heating rate and while an exothermic peak associated with cocrystal formation was not necessarily confirmed, we were able to detect the exothermic peak by changing the heating rate. These experimental observations clarified the relationship between the thermal behavior of a physical mixture and cocrystal formation. When high-throughput preparation of a homogeneously-mixed fine physical mixture is achieved, an efficient cocrystal 'CCF' screening system may be available using DSC equipped with an auto-sampling attachment.

## ACKNOWLEDGMENTS AND DISCLOSURES

We thank Toshikazu Adachi for supporting our experiments and Mayuko Mirun for assisting in conducting the experiments.

## REFERENCES

1. Jones W, Motherwell S, Trask AV. Pharmaceutical cocrystals: an emerging approach to physical property enhancement. MRS Bull. 2006;31(11):875–9.
2. Bhogala BR, Nangia A. Ternary and quaternary co-crystals of 1,3-cis,5-cis-cyclohexanetricarboxylic acid and 4,4′-bipyridines. New J Chem. 2008;32(5):800–7.
3. Stahly GP. Diversity in single- and multiple-component crystals. The search for and prevalence of polymorphs and cocrystals. Cryst Growth Des. 2007;7(6):1007–26.
4. Aakeroy CB, Forbes S, Desper J. Using cocrystals to systematically modulate aqueous solubility and melting behavior of an anticancer drug. J Am Chem Soc. 2009;131(47):17048–9.
5. Remenar JF, Morissette SL, Peterson ML, Moulton B, MacPhee JM, Guzman HR, *et al.* Crystal engineering of novel cocrystals of a triazole drug with 1,4-dicarboxylic acids. J Am Chem Soc. 2003;125(28):8456–7.
6. Good DJ, Rodriguez-Hornedo N. Solubility advantage of pharmaceutical cocrystals. Cryst Growth Des. 2009;9(5):2252–64.
7. Trask AV, Motherwell WDS, Jones W. Physical stability enhancement of theophylline *via* cocrystallization. Int J Pharm. 2006;320 (1–2):114–23.
8. Trask AV, Motherwell WDS, Jones W. Pharmaceutical cocrystallization: engineering a remedy for caffeine hydration. Cryst Growth Des. 2005;5(3):101–21.
9. Karki S, Friscic T, Fabian L, Laity PR, Day GM, Jones W. Improving mechanical properties of crystalline solids by cocrystal formation: new compressible forms of paracetamol. Adv Mater. 2009;21:3905–9.
10. Sun CC, Hou H. Improving mechanical properties of caffeine and methyl gallate crystals by cocrystallization. Cryst Growth Des. 2008;8(5):1575–9.
11. McNamara DP, Childs SL, Giordano J, Iarriccio A, Cassidy J, Shet MS, *et al.* Use of a glutaric acid cocrystal to improve oral bioavailability of a low solubility API. Pharm Res. 2006;23(8):1888–97.
12. Hickey MB, Peterson ML, Scoppettuolo LA, Morrisette SL, Vetter A, Guzman H, *et al.* Performance comparison of a co-crystal of carbamazepine with marketed product. Eur J Pharm Biopharm. 2007;67(1):112–9.
13. Chadwick K, Davey RJ, Dent G, Pritchard RG, Hunter CA, Musumeci D. Cocrystallization: a solution chemistry perspective and the case of benzophenone and diphenylamine. Cryst Growth Des. 2009;9(4):1990–9.
14. Jayasankar A, Reddy LS, Bethune SJ, Rodriguez-Hornedo N. Role of cocrystal and solution chemistry on the formation and stability of cocrystals with different stoichiometry. Cryst Growth Des. 2009;9(2):889–97.
15. Takata N, Shiraki K, Takano R, Hayashi Y, Terada K. Cocrystal screening of stanolone and mestanolone using slurry crystallization. Cryst Growth Des. 2008;8(8):3032–7.
16. Zhang GGZ, Henry RF, Borchardt TB, Lou XC. Efficient co-crystal screening using solution-mediated phase transformation. J Pharm Sci-Us. 2007;96(5):990–5.
17. Weyna DR, Shattock T, Vishweshwar P, Zaworotko MJ. Synthesis and structural characterization of cocrystals and pharmaceutical cocrystals: mechanochemistry vs slow evaporation from solution. Cryst Growth Des. 2009;9(2):1106–23.
18. Basavoju S, Bostrom D, Velaga SP. Indomethacin-saccharin cocrystal: design, synthesis and preliminary pharmaceutical characterization. Pharm Res. 2008;25(3):530–41.
19. Trask AV, van de Streek J, Motherwell WDS, Jones W. Achieving polymorphic and stoichiometric diversity in cocrystal formation: importance of solid-state grinding, powder X-ray structure determination, and seeding. Cryst Growth Des. 2005;5(6):2233–41.
20. Shan N, Toda F, Jones W. Mechanochemistry and co-crystal formation: effect of solvent on reaction kinetics. Chem Commun. 2002;20:2372–3.
21. Trask AV, Jones W. Crystal engineering of organic cocrystals by the solid-state grinding approach. Org Solid State React. 2005; 254:41–70.
22. Aher S, Dhumal R, Mahadik K, Paradkar A, York P. Ultrasound assisted cocrystallization from solution (USSC) containing a non-congruently soluble cocrystal component pair: caffeine/maleic acid. Eur J Pharm Sci. 2010;41(5):597–602.
23. Chadwick K, Davey R, Cross W. How does grinding produce co-crystals? Insights from the case of benzophenone and diphenylamine. CrystEngComm. 2007;9(9):732–4.
24. Berry DJ, Seaton CC, Clegg W, Harrington RW, Coles SJ, Horton PN, *et al.* Applying hot-stage microscopy to co-crystal screening: a study of nicotinamide with seven active pharmaceutical ingredients. Cryst Growth Des. 2008;8(5):1697–712.
25. Dhumal RS, Kelly AL, York P, Coates PD, Paradkar A. Cocrystalization and simultaneous agglomeration using hot melt extrusion. Pharm Res. 2010;27(12):2725–33.
26. Castellan GW. Physical chemistry. 3rd ed. San Francisco: Benjamin Cummings Pub. Co.; 1983.
27. Singh NB, Das SS, Gupta P, Dwivedi MK. Phase equillibria and solidification behaviour in the vanillin-p-anisidine system. J Cryst Growth. 2008;311(1):118–22.
28. Dwivedi Y, Kant S, Rai SB, Rai RN. Synthesis, physicochemical and optical characterization of novel fluorescing complex: o-phenylenediamine-benzoin. J Fluoresc. 2011;21(3):1255–63.
29. Rai US, George S. Thermochemical studies on the eutectics and addition-compounds in the binary-systems of benzidine with P-nitrophenol, M-aminophenol and resorcinol. Thermochim Acta. 1994;243(1):17–25.
30. Crowley KJ, Forbes RT, York P, Nyqvist H, Camber O. Oleate salt formation and mesomorphic behavior in the propranolol oleic acid binary system. J Pharm Sci-Us. 1999;88(6):586–91.
31. Winfield AJ, Saidan SHA. Compound formation in phenobarbitone-urea systems. Int J Pharm. 1981;8:211–6.
32. Grant DW, Jacobson H, Fairbrother JE, Patel CG. Phases, in the paracetamol-phenazone system. Int J Pharm. 1980;5:109–16.
33. Lu E, Rodriguez-Hornedo N, Suryanarayanan R. A rapid thermal method for cocrystal screening. Cryst Eng Comm. 2008;10(6): 665–8.
34. Sangster J. Phase diagrams and thermodynamic properties of binary systems of drugs. J Phys Chem Ref Data. 1999;28(4):889–930.
35. Bhatt PM, Ravindra NV, Banerjee R, Desiraju GR. Saccharin as a salt former. Enhanced solubilities of saccharinates of active pharmaceutical ingredients. Chem Commun. 2005;28(8):1073–5.
36. Childs SL, Rodriguez-Hornedo N, Reddy LS, Jayasankar A, Maheshwari C, McCausland L, *et al.* Screening strategies based on solubility and solution composition generate pharmaceutically acceptable cocrystals of carbamazepine. Cryst Eng Comm. 2008;10 (7):856–64.
37. Fleischman SG, Kuduva SS, McMahon JA, Moulton B, Walsh RDB, Rodriguez-Hornedo N, *et al.* Crystal engineering of the composition of pharmaceutical phases: multiple-component crystalline solids involving carbamazepine. Cryst Growth Des. 2003;3(6):909–19.
38. Jayasankar A, Somwangthanaroj A, Shao ZJ, Rodriguez-Hornedo N. Cocrystal formation during cogrinding and storage is mediated by amorphous phase. Pharm Res. 2006;23(10):2381–92.